

A Wearable System for Electrodermal Activity Data Acquisition in Collective Experience Assessment

Patrícia Bota¹ , Chen Wang², Ana Fred¹  and Hugo Silva¹ 

¹*Instituto Superior Técnico, Department of Bioengineering & Instituto de Telecomunicações,
Av. Rovisco Pais n. 1, Torre Norte - Piso 10, 1049-001 Lisboa, Portugal*

²*Future Media & Convergence Institute (FMCI), Xinhua Net, Jinxuan Building,
No. 129 Xuanwumen West Street, Beijing 100031, China*

Keywords: Electrodermal Activity Response, Wearable Sensors, Physiological Data, Signal Processing.


Abstract: In the recent years, we have been observing an increase of research work involving the use of biomedical data in affective computing applications, which is ever more dependent on data and its quality. Many physiological data acquisition devices have been developed and validated. However, there is still a need for pervasive and unobtrusive equipment for collective synchronised acquisitions. In this work, we introduce a novel system, the Electrodermal Activity (EDA) Xinhua Net Future Media Convergence Institute (FMCI) device, allowing group data acquisitions, and benchmark its performance using the established BITalino as gold standard. We developed a methodical experimental protocol in order to acquire data from the two devices simultaneously, and analyse their performance over a comprehensive set of criteria – Data Quality Analysis. Additionally, the FMCI data quality is assessed over five different setup scenarios towards its validation in a real-world scenario – Data Loss Analysis. The experimental results show a close similarity between the data collected by both devices, paving the way for the application of the proposed equipment in simultaneous, collective data acquisition use cases.


1 INTRODUCTION


The field of Affective Computing focuses on the computing that relates to, arises from, or influences emotions (Picard, 1997). The field encompasses many applications, such as the analysis in real-time of the collective response of an audience during a theatrical play or show. Collective responses can be applied to: (1) Testing a group in order to gauge the content marketing success; (2) Direct an artist into new performing/narrative concepts, leading to futuristic mechanism where the content narrative adapts to the audience response; (3) Enhance remote distributed systems, creating feedback channels so the actors are in contact with the audience and aware of their response, and the audience feels immersed and not like it is watching a recorded video instead of a live performance, (Wang, 2018); (4) Create personalised list content recommendations; (5) Enhance health applications, and many others.

However, in order to gauge the collective response, researchers need pervasive and unobtrusive physiological sensors (Bota et al., 2019). Although many have been developed and validated (Abreu, 2020), for group settings, such as a theatre or cinema, there is a need in the literature for devices able to perform data collection from a group, using several devices synchronously and simultaneously.

Therefore, in this work we: (1) Introduce the Xinhua Net Future Media Convergence Institute (FMCI) device containing a Electrodermal Activity (EDA) embedded sensor, describing the hardware development path throughout its various versions, which culminated in an architecture capable of acquiring EDA data with quality at least of 20 devices in simultaneously; (2) Validate the device performance, ensuring its scalability in a real-world scenario, against BITalino, a well-established and recognised system that we consider as a gold standard. The BITalino device has been independently recognised as the most prospective physiological pervasive wearable device for heart rate (HR) and EDA measurements in affective computing applications (Batista et al., 2019; Kutt et al., 2018). To accomplish this task, we follow an experimental

^a  <https://orcid.org/0000-0002-0514-7517>

^b  <https://orcid.org/0000-0003-1320-5024>

^c  <https://orcid.org/0000-0001-6764-8432>

protocol to acquire data from the two devices simultaneously – Data Quality Analysis –, and compare the obtained data using a diverse set of metrics on the signal morphological structure, Power Spectrum (R^2 -score, Pearson Correlation (PC), Root Mean Square Error (RMSE), Dynamic Time Warping (DTW) distance), and EDA – specific events to benchmark the performance of the FMCI device. Lastly, we perform a set of experiments to assess the FMCI device data quality under five different setup conditions towards the validation of its performance in a real-world scenario – Data Loss Protocol.

The remainder of this paper is organised as follows: In Section 2, we introduce the BITalino and the FMCI devices, and present a summary of the EDA signal. In Section 3, we describe the data acquisition protocol and, lastly, briefly depict the metrics we use as evaluation criteria to compare both sensors' signals. In Section 4, we present and discuss the experimental results; and finally, in Section 5, we outline the main conclusions, along with future work directions.

2 BACKGROUND

In this section, we introduce the EDA sensor data, the BITalino and FMCI devices, and describe the FMCI hardware development path throughout its versions.

2.1 Electrodermal Activity Signal

The EDA typically measures the skin resistance by applying a negligible current/voltage and reading the voltage/current variation output between the two sensor leads ($G = 1/R$; $R = V/I$). This is based on the principle that the electrical properties of the skin change with the psychophysiological activity of the user (Boucsein, 2012). Moreover, the EDA signal is characterised by a baseline tonic component – Electrodermal Level (EDL) – expressing the baseline and thermal regulation activities, from which phasic variations arise from psychological-related responses. The latter is denoted as the Electrodermal Response (EDR) signal, derived from the increase/decrease of perspiration, piloerection, and vasomotor changes elicited by various emotional states via the limbic system. Figure 1 displays an example of an EDA signal.

Sweat is highly conductive, thus, modifies the skin resistance as a result of secretion / inhibition. For this reason, the EDA electrodes are usually placed at areas of high sweat gland density, such as on the 2nd phalanx of the index and middle fingers, the index and ring fingers, the hand, or feet soles (Schmidt et al., 2019). Since the EDA can be used as a non-intrusive window

into the ANS activity, it is widely used in biomedical research for example in diagnostic (Poh et al., 2010), or emotion recognition (Shukla et al., 2019), polygraph tests, or stress/relaxation biofeedback.

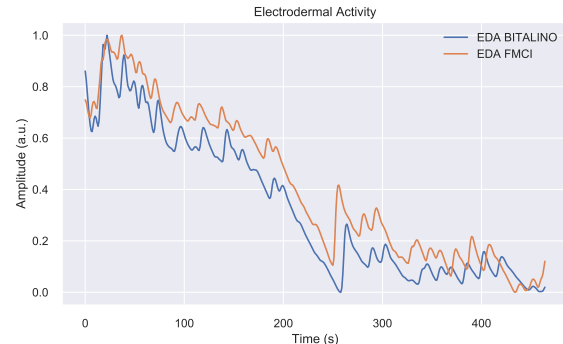


Figure 1: Signal trace for the FMCI and BITalino devices.

2.2 FMCI Hardware Development Path

The FMCI EDA sensor is based on a operational trans-conductance amplifier (OTA) and a low-pass filter (LPF). The former is used to increase the amplitude of the weak potential differences generated from the biological electric signals. The OTA is ideal for measuring signals from low level output transducers in noisy environments, amplifying the difference between two input signal voltages, and rejecting any signals that are common to both input terminals, thus reducing the undesired source errors. This is known as Common-Mode Rejection Ratio (CMRR). The typical effective frequency for the EDA sensors has been characterized in the state-of-the-art to be between 0.01-1 Hz (Boucsein, 2012). Nevertheless, after the OTA, a second order low-pass Butterworth filter (gain = 2, cut-off frequency = 5Hz) is applied to remove the frequencies that lie outside the defined range. So far, four prototype versions (Figure 2) have been explored through a continuous development cycle consisting of a thorough analysis of environment testing, user experience and sensor performance, which we detail below:

- **Version 1.** It was developed using Arduino boards, Xbee wireless transmitters, and filters – built with resistors and capacitors to reduce noise interference. The measurement system consisted of 15 EDA sensors, 3 Arduino boards and 4 Xbee modules. Each Arduino board (1 Hz sampling rate) carrying 5 EDA sensors uses one Xbee module to send data to a Xbee coordinator, connected to a laptop server. The Xbee coordinator applies a polling scheme to receive packets from the different Arduino boards in order to minimise packet loss ratio in the wireless communication channel. Some lim-

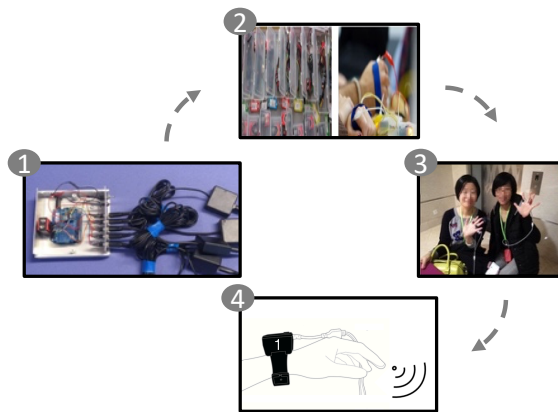


Figure 2: The hardware development path showing generation 1 (left), 2 (top), 3 (right), and 4 (bottom).

iterations were found in the first generation sensor, namely: it was not wearable, nor comfortable for the users to use for a long time; the communication range (10-20 meters) was rather short for a system to be used in a collective environment; the battery consumption was very high, being exhausted after roughly half an hour of use.

- Version 2.** The JeeNode was selected for the development board, as it was small, economic, and can communicate using the 915 MHz, 868 MHz or 433 MHz band. As a result, the system integrated with the JeeNode was much smaller and more economical than Version 1. The standard Lithium Polymer battery (1100 mAh, 3.7 voltage) supported the JeeNode attached with one EDA sensor (sampling rate: 10 Hz) to work for over 50 hours. Besides, the JeeNode supported up to 250 different groups, each with up to 30 different node IDs. This meant that large groups could be monitored simultaneously. However, the second version still showed some limitations in a collective environment: the users did not feel comfortable in terms of sensor housing and the electrodes; the soldering work in the lab did not yield reliability when sensors were used in reality; some mechanical wires in the system design created some connection problems in the experiments.
- Version 3.** It initiated the industrialisation of the device. Two versions were produced: one for adults, and one for children. These sensors were rather small, and each was fitted in a 3D printed box of 10x5x2 cm. The EDA sensors produced by the factory could ensure that the quality was robust and reliable. However, this version was shown not to be convenient for experimental operators. Moreover, taking off/putting on a sensor housing when testing a sensor, required high effort. In addition,

there was no way for the operators to monitor the working states of the sensors.

- Version 4.** In the current version, the circuit design was upgraded, and the sensor housing was removed. The circuit was first prototyped on a breadboard and connected to the JeeNode board. After that, an EDA board was produced to obtain a compact EDA sensor with the interfaces needed by the JeeNode board. The JeeNode board and EDA sensor were connected and mounted in a customized box produced by laser cutting. Two electrodes were connected via a cable. In this way, operators could easily take off the sensor housing, and test the sensor boards. Additionally, in this version, a monitoring system to observe the working state of the EDA sensor was developed. In this way, it could be seen which node is working or not, so that it could be fixed or replaced.

2.3 Devices Overview

To evaluate the proposed device, we compare the FMCI sensor performance against the BITalino (r)evolution (Batista et al., 2019).

Regarding the BITalino device, for the data acquisition, the OpenSignals (r)evolution software¹ was used. On the other hand, for the FMCI device, a data logger was developed by the authors, which we made publicly available². In both devices, the data was transmitted wirelessly, and a 2-lead accessory was used during the data acquisition. Table 1 presents some of the devices main specifications; no further information was found on the Xinhua Net device.

Table 1: BITalino and FMCI device specifications.

	BITalino	FMCI
Measurement Range	0-25 μ S (with VCC = 3.3V)	
Bandwidth	0-2.8Hz	0-5Hz
Consumption	~0.72mA	
Input Voltage Range	1.8-5.5V	
Sampling Frequency	1000Hz	1Hz

3 METHODS

In this section, we outline the overall methodology we followed for the benchmark of the FMCI device.

3.1 Data Quality Protocol

As explained in Section 2.1, the EDA sensors measure the body sympathetic nervous system (SNS) activity

¹<https://bitalino.com/en/software>

²<https://github.com/PIA-Group/python-fmci-datalogger-example>

through the skin resistance/conductance. To promote reflex responses and enable the benchmarking of the devices, we devised an acquisition protocol performing an isometric handgrip test, a common state-of-the-art clinic test to elicit reflex SNS responses (Hilz and Dütsch, 2006; Zygmunt and Stanczyk, 2010). During the acquisition, the subjects were asked to remain seated while an isometric grip test was performed for 5 min. Each experiment was carried according to the following protocol:

1. **Sensors Placement.** Application of the FMCI wearable, FMCI and BITalino electrodes. To avoid cross-talk between the two devices, FMCI electrodes were placed on the index finger and BITalino's were attached to the ring finger.
2. **Isometric Handgrip Test.** The subject squeezed a hand handgrip dynamometer at his maximum contraction strength (calibration) and then had to maintain above two-third of the maximum contraction strength for 5 min. The GripIT application (Costa et al., 2019) was connected to a force sensor and used by the subject to help them keep control of the exerted force.

The aforementioned acquisition protocol was performed by 15 subjects with ages 18 to 24 years old. Three acquisitions were discarded. To synchronise both devices, a BITalino Light (LUX) sensor was used to capture the pulse emitted when the FMCI device was turned on and turned off, i.e. when the device started and stopped acquiring data.

3.2 Data Loss Protocol

Additionally, to evaluate the FMCI device in group acquisitions, a test when multiple units are collecting data simultaneously was performed for five different environment conditions:

- **Test 1 – 20 Devices in Simultaneous Acquisition (60-min).** The device's placement is displayed in Figure 3. As it can be seen, the antenna was placed so it was in the direct line of the centre of the devices.

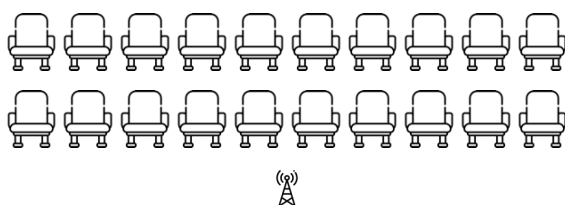


Figure 3: Devices and antenna placement setup for Test 1 – 20 devices in simultaneous acquisition.

- **Test 2 – 10 Devices in Simultaneous Acquisition (30-min).** In the second experiment, the number of devices was reduced from 20 to 10, acquiring data simultaneously, simulating a smaller audience. The antenna was moved, so it continued to be placed in the centre of the devices' group.
- **Test 3 – 20 Devices at Different Ranges to the Antenna (20-min).** With the same disposition as Test 1, the antenna was moved in order to be at a distance of: 270, 450, 630, and 900 cm to the centre line of the devices.
- **Test 4 – Occlusion (20-min).** In order to evaluate the occlusion by the human body, two subjects sat side-by-side, wearing one device in each hand.
- **Test 5 – Random Movement (10-min).** The last test consisted of the replication of common movement artefacts such as: putting the bracelet on, random movement, touching the nose and hair, clapping, and taking the bracelet off.

3.3 Signal Pre-processing

The EDA data can be corrupted by powerline interference, thus, in order to remove the noise, a low-pass filter with 4Hz cut-off frequency was applied to the BITalino device data. As stated in Section 2.3, the BITalino has a sampling frequency of 1000Hz and the FMCI device of 1Hz, therefore, a downsampling to 1Hz was performed using cubic interpolation. The data was then passed through a smoothing filter.

Since scale-dependent metrics were going to be obtained, and, to remove subjective bias, the data was normalised per user to values between [0; 1] by $X_{scaled} = \frac{X - X_{min}}{X_{max} - X_{min}}$.

3.4 Performance Evaluation Metrics

In order to compare the waveform similarity of both devices, we resorted to the following criteria:

- **Coefficient of Determination (R²-Score)** (Ross, 2010): consist of the percentage of variation explained the correlation between the dependent and the independent variables. The R² score is given by: $R^2 = 1 - \frac{\sum_i (y_i - \hat{y}_i)^2}{\sum_i (y_i - \bar{y})^2}$. Where, y consists on the observed data, \bar{y} its mean value, and \hat{y} the predicted value at data point $i \in \{0, \dots, N\}$; N being the total number of data points. It presents a range between negative values and a maximum value of 1 – for the utmost best score. Thus, a value of R² equal to 1 indicates that the model is able to explain 100% of the variation of the data, while a value of R² near 0, indicates that the variance of the output is

mostly due to error random variables. The R^2 score is largely used in literature to evaluate regression models.

- **Pearson Correlation** (Kirch, 2008): measures the linear correlation between two variables, given by:

$$\rho = \frac{\sum_{i=1}^n (x_i - \hat{x})(y_i - \hat{y})}{\sqrt{\sum_{i=1}^n (x_i - \hat{x})^2} \cdot \sqrt{\sum_{i=1}^n (y_i - \hat{y})^2}}$$
. Where x_i and y_i represent two samples indexed at i ; n the sample size and \hat{x} , \hat{y} , the x and y variables sample mean, respectively. It presents a value between $+1$ and -1 , where a value of 1 denotes total positive correlation, 0 no linear correlation, and -1 , total linear correlation with a negative slope.

- **Root Mean Squared Error (RMSE)** (Neill and Hashemi, 2018): consists of the aggregation of the magnitude of the predicted errors, through the square root of the second sample moment of the differences between the predicted values and the observed values. It is given by: $RMSE = \sqrt{\frac{\sum_{i=1}^n (y_i - \hat{y}_i)^2}{n}}$. Where \hat{y}_i is the predicted value at index i , y_i the sample value, and n the sample size. It presents non-negative values, with 0 denoting a perfect fit of the model to the data.

- **Dynamic Time Warping (DTW)** (Niels, 2004): measures the Euclidean distance optimal alignment between two time series. The optimal alignment (warping path) consists of the minimum value in the $N \times M$ cost matrix given by $C(S_1, S_2)$, where $S_1 := \{s_{11}, s_{12}, \dots, s_{1N}\}$, and $S_2 := \{s_{21}, s_{22}, \dots, s_{2M}\}$ are two time series of length N and M ; $N, M \in \mathbb{N}$, respectively. The parameter $C(S_1, S_2)$, yields a small value (low cost) if S_1 and S_2 are similar, and a larger value (high cost), otherwise.

4 RESULTS

In this section, we first present a morphological and event-based comparison analysis between the FMCI and BITalino devices (Data Quality Protocol in Subsection 3.1). Then, we show an analysis of the FMCI device data quality over five different environment setups in order to evaluate its deployment in real-world scenarios (Data Loss Protocol in Subsection 3.2).

Data Quality Results. Table 2 and Table 3 show the experimental results for the Data Quality Protocol described in Section 3.1.

- **EDA Morphology.** In Table 2, we observe that both devices attain a reasonable correlation (0.65 ± 0.28), displaying a very low value RMSE (0.19

Table 2: Experimental results for the morphological comparison between the data from the two devices in terms of Pearson Correlation (PC); Root Mean Squared Error (RMSE); R^2 -score; and Dynamic Time Warping (DTW) distance. Nomenclature: EDA- Electrodermal Activity; EDR- Electrodermal Response.

	EDA Morphology	EDR Morphology	Power Spectrum
PC	0.65 ± 0.28	0.15 ± 0.28	0.81 ± 0.07
RMSE	0.19 ± 0.06	0.20 ± 0.03	0.14 ± 0.04
R^2 -score	0.54 ± 0.39	0.99 ± 0.65	0.42 ± 0.25
DTW	0.06 ± 0.49	0.09 ± 0.04	0.05 ± 0.03

Table 3: Experimental results for the detection of events for the BITalino and FMCI devices in terms of: number of events (N° of Events), offset between the number obtained in both devices.

N° of Events	EDA	EDR
BITalino	19.1 ± 7.0	34.6 ± 13.0
FMCI	18.5 ± 7.4	31.9 ± 12.4
Offset	3.4 ± 2.5	5.8 ± 5.0

± 0.06), reasonable R^2 -score (0.54 ± 0.39), and very low DTW distance (0.06 ± 0.49). Thus, indicating a high morphological correlation between the data acquired by the two devices.

- **EDR Morphology.** Regarding the EDR morphology, the Pearson correlation decreases in comparison to the EDA morphology analysis (0.15 ± 0.28), the RMSE and the DTW distance maintain their low values (0.20 ± 0.03 , and 0.09 ± 0.04 , respectively), and the R^2 -score increases to nearly 1 . Therefore, although the high-frequency content of the EDA corrupts the EDR information which results in the detriment of the Pearson correlation, both signals still maintain high correlation.
- **Power Spectrum.** Additionally, for the power spectrum the correlation is very high (0.81 ± 0.07), with very low RMSE and DTW distance (0.14 ± 0.04 , and 0.05 ± 0.03 , respectively), therefore, denoting a very high spectral correlation between both devices signals. The R^2 -score, is the lowest from all the representations, possibly due to the power spectrum being a very noisy signal with low linear dependency.
- **EDA Signal Characteristics.** Table 3 shows that the EDA morphology, in the BITalino data obtained 19.1 ± 7.0 events, while in the FMCI device 18.5 ± 7.4 events were found, thus resulting in an offset of 3.4 ± 2.5 events. On the other hand, for the EDR morphology, in the BITalino data we obtained 34.6 ± 13.0 events, while for the FMCI device we observed 31.9 ± 12.4 events.

We can conclude that overall a similar number of

events is detected in both devices, with the exception of a few users that present higher discrepancy, augmenting the standard deviation and introducing bias. Better results would be expected if both devices were locally and synchronised in time, i.e. the data were obtained in the same body localisation, and perfectly timely synchronised. By an empirical observation of the data, overall, we also highlight that the same morphological trends were noticed in both devices' data, however, with magnitude offsets and time warping issues. This can also explain some of the discrepancies in results.

Data Loss Results. In this subsection, we present the results for the five experiments in the Data Loss Protocol described in Section 3.2.

- **Test 1 – 20 Devices in Simultaneous Acquisition.** The experimental results showed that only devices 109 and 110 exhibited transmission errors. The devices were placed in the same chair, close to each other, so interference could have caused the malfunctioning. Device 110 displays the higher error rate, with a value of 0.12 errors/s, while device 109 presents an error rate of 0.01 errors/s; the remaining devices (18 devices) returned no errors. Additionally, a timeline view of the errors shows that these were systematic; i.e. consistent throughout the acquisition.
- **Test 2 – 10 Devices in Simultaneous Acquisition.** During the second experiment, the error rate of device 110 persisted with a similar value (approximately 0.12 errors/s). However, new devices (107, 111), started to return errors. The device 109 displayed an error rate of 0.2 errors/s, while device 111 an error rate of around 0.1 errors/s. Once again, the errors were consistent throughout the experiment.
- **Test 3 – 20 Devices at Different Ranges to the Antenna.** The results for a distance between the devices and the router of 270, 450, 630, and 900 cm are displayed in Figure 4 to Figure 11, in Appendix. In the timeline view of the errors, as for the previous experiences, the error rate was consistent throughout the acquisition protocol. At the first distance (270 cm), closer to the antenna, devices 109 and 110, on the whole, maintained their error rate. A new device, device 115, started to display errors, with a high error rate (approximately 1.5 errors/s). At the second distance iteration (450 cm), the devices returning an error were maintained, however, the error rate from each decreased. Next, for the third distance iteration (630 cm), the number of devices displaying errors increased to 6. The

error rate in the devices showing errors at the previous iteration expanded significantly. At the fourth distance iteration (900 cm), a higher number of devices have shown data loss (9 devices) with error rates from 0.1 to 1.3 errors/s.

- **Test 4 – Occlusion.** In a 20-minute experience, no errors were obtained. Consequently, we can conclude that body occlusion did not increase the number of the devices' errors.
- **Test 5 – Random Movement.** Only one device displayed errors, with an error rate of 0.08 errors/s. Once again, the errors were consistent throughout the experiment.

To conclude, after analysing the five setup experiments, the FMCI device shows suitability to be used in simultaneous collective acquisitions, showing acceptable packet loss.

5 CONCLUSION

Recent advances in wearable technology and its proliferation into people's daily living lead to a diversity of devices focused on the acquisition of physiological data. Additionally, we have been observing a transformation in entertainment, bringing new challenges and possibilities to media providers and content creators. Physiological data, namely the EDA, can be used to measure an audience response and provide meaningful information for both the audience, the artist and producers, paving the way for futuristic shows and entertainment experiences, in both co-located or distributed setting. Still, there are few practical options for simultaneous data acquisition (e.g. in an audience setting).

In this work, we (1) Introduce a new wearable device for EDA sensing, the Xinhua Net FMCI device, which expands the current state-of-the-art by allowing collective, simultaneous acquisition of data; (2) Evaluate its performance against the BITalino device, a reference and recognised system. In order to perform this task, we follow two protocols: (1) Data Quality Protocol – replicating a methodological experiment based on a common state-of-the-art test to elicit the SNS activity, namely the isometric handgrip test; (2) Data Loss Protocol – examining the device packet loss during five different setup conditions.

In both protocols, the devices showed high similarity between the acquired data, and no significant data loss was observed in a collective setting with multiple devices acquiring data simultaneously and synchronously. Therefore, we can conclude its applicability for future research in collective data acquisition

experiences.

Given the experimental results, we identified the following research lines for further work: (1) Addition of further sensor modalities such as ECG, BVP or HR; (2) Addition of a button or auxiliary channel for synchronisation to further enhance the research applicability; (3) Development of an online interface for real-time visualisation of the data; (4) Data quality index calculation, returning the usability/quality of the data; (5) Increase of the sampling rate; (6) Application of anonymization and data-privacy methodologies; (7) Validation of the FMCI device over well-known data and information-quality frameworks.

ACKNOWLEDGEMENTS

This work has been partially funded by the Xinhua Net Future Media Convergence Institute under project S-0003-LX-18, by the Ministry of Economy and Competitiveness of the Spanish Government co-founded by the ERDF (PhysComp project) under Grant TIN2017-85409-P, and by IT - Instituto de Telecomunicações in the scope of program UIDB/50008/2020. The authors would also like to thank to Carolina Bento for the support to the experimental part of the work, and to all the volunteers that participated in the Data Quality Protocol.

REFERENCES

- Abreu, M. (2020). A review of wearables and related devices applicable to epileptic seizure prediction via peripheral measurements. Technical Report #IT-FMCI-20190905, IT - Instituto de Telecomunicações.
- Batista, D., da Silva, H. P., Fred, A., Moreira, C., Reis, M., and Ferreira, H. (2019). Benchmarking of the BITalino biomedical toolkit against an established gold standard. *Healthcare Technology Letters*, 6(1):32–36.
- Bota, P. J., Wang, C., Fred, A. L. N., and Plácido Da Silva, H. (2019). A review, current challenges, and future possibilities on emotion recognition using machine learning and physiological signals. *IEEE Access*, 7:140990–141020.
- Boucsein, W. (2012). *Principles of Electrodermal Phenomena*, pages 1–86. Springer US, Boston, MA.
- Costa, P. F., Rocha, M., Baptista, R., and Silva, H. (2019). GripIT: A mobile isometric handgrip test for evaluation of autonomic cardiovascular reflexes in non-clinical applications. In *Int'l. Conf. of the IEEE Eng. in Medicine and Biology Society*.
- Hilz, M. J. and Dütsch, M. (2006). Quantitative studies of autonomic function. *Muscle & Nerve*, 33(1):6–20.
- Kirch, W. (2008). *Pearson's Correlation Coefficient*, pages 1090–1091. Springer Netherlands, Dordrecht.

- Kutt, K., Binek, W., Misiak, P., Nalepa, G., and Bobek, S. (2018). Towards the development of sensor platform for processing physiological data from wearable sensors. In *Int'l Conf. on Artificial Intelligence and Soft Computing*, pages 168–178.
- Neill, S. P. and Hashemi, M. R. (2018). Ocean modelling for resource characterization. In Neill, S. P. and Hashemi, M. R., editors, *Fundamentals of Ocean Renewable Energy*, pages 193 – 235. Academic Press.
- Niels, R. (2004). Dynamic time warping: An intuitive way of handwriting recognition?
- Picard, R. W. (1997). *Affective Computing*. MIT Press, Cambridge, MA, USA.
- Poh, M., Loddenkemper, T., Swenson, N. C., Goyal, S., Madsen, J. R., and Picard, R. W. (2010). Continuous monitoring of electrodermal activity during epileptic seizures using a wearable sensor. In *Int'l Conf. of the IEEE Eng. in Medicine and Biology*, pages 4415–4418.
- Ross, S. M. (2010). Linear regression. In Ross, S. M., editor, *Introductory Statistics*, pages 537 – 604. Academic Press, Boston.
- Schmidt, P., Reiss, A., Dürichen, R., and Laerhoven, K. V. (2019). Wearable-based affect recognition—a review. *Sensors*, 19(19).
- Shukla, J., Barreda-Angeles, M., Oliver, J., Nandi, G. C., and Puig, D. (2019). Feature extraction and selection for emotion recognition from electrodermal activity. *IEEE Tran on Affective Computing*, pages 1–1.
- Wang, C. (2018). *Monitoring the Engagement of Groups by Using Physiological Sensors*. PhD thesis, Vrije Universiteit Amsterdam.
- Zygmunt, A. and Stanczyk, J. (2010). Methods of evaluation of autonomic nervous system function. *Archives of medical science : AMS*, 6(1):11–18.

APPENDIX

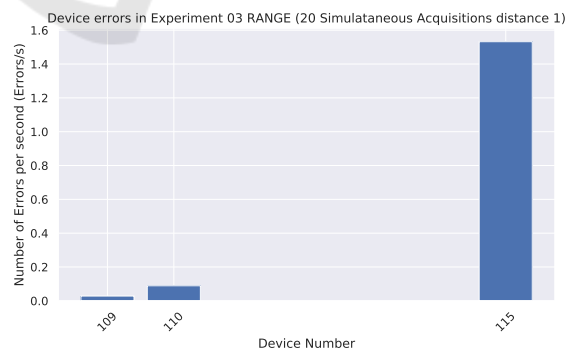


Figure 4: Number of errors per device for Test 3 – 20 devices in simultaneous acquisition at a 270 meter distance.

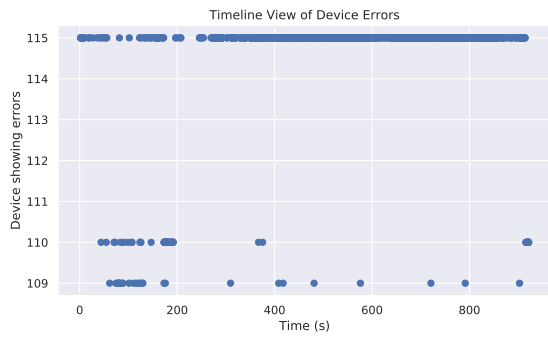


Figure 5: Timeline view of the devices' errors for Test 3 – 20 devices in simultaneous acquisition at a 450 meter distance.

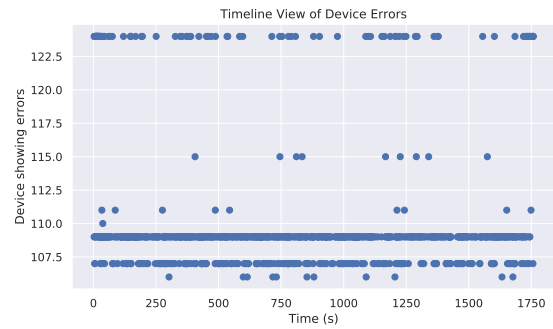


Figure 9: Timeline view of the devices' errors for Test 3 – 20 devices in simultaneous acquisition at a 630 meter distance.

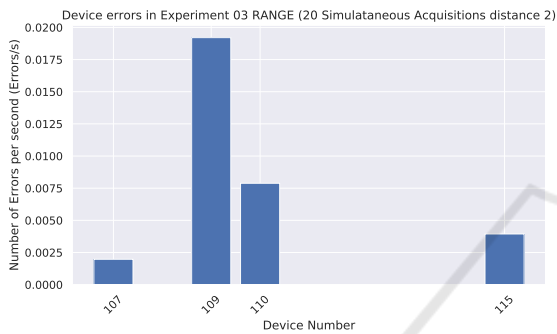


Figure 6: Number of errors per device for Test 3 – 20 devices in simultaneous acquisition at a 270 meter distance.

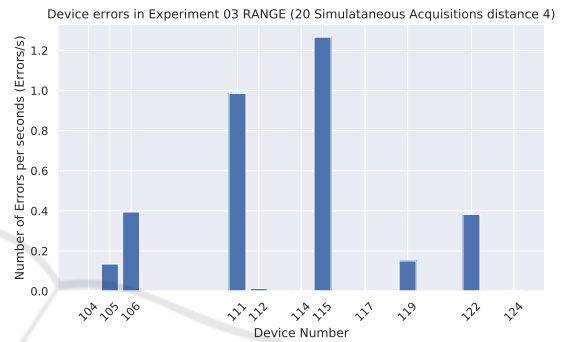


Figure 10: Number of errors per device for Test 3 – 20 devices in simultaneous acquisition at a 900 meter distance.

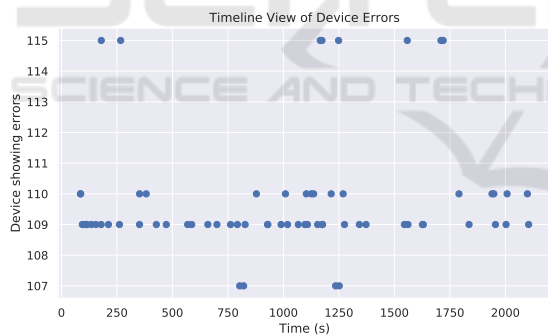


Figure 7: Timeline view of the devices' errors for Test 3 – 20 devices in simultaneous acquisition at a 450 meter distance.

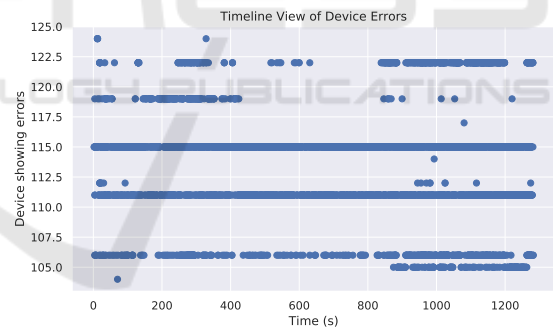


Figure 11: Timeline view of the devices' errors for Test 3 – 20 devices in simultaneous acquisition at a 900 meter distance.

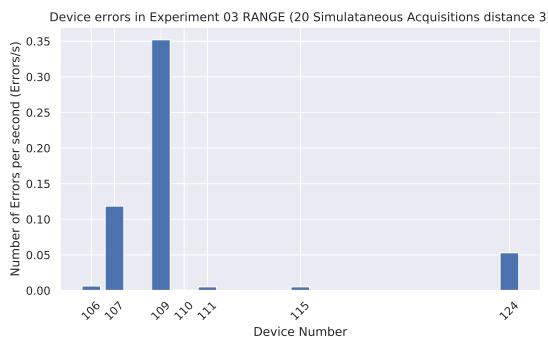


Figure 8: Number of errors per device for Test 3 – 20 devices in simultaneous acquisition at a 630 meter distance.